

AFRL-VA-WP-TP-2007-311

**A REVIEW OF RECENT ALGORITHMS
AND A NEW AND IMPROVED
COOPERATIVE CONTROL DESIGN FOR
GENERATING A PHANTOM TRACK
(PREPRINT)**



Keith B. Purvis and Phillip R. Chandler

FEBRUARY 2007

Approved for public release; distribution unlimited.

STINFO COPY

This is a work of the U.S. Government and is not subject to copyright protection in the United States.

**AIR VEHICLES DIRECTORATE
AIR FORCE MATERIEL COMMAND
AIR FORCE RESEARCH LABORATORY
WRIGHT-PATTERSON AIR FORCE BASE, OH 45433-7542**

NOTICE AND SIGNATURE PAGE

Using Government drawings, specifications, or other data included in this document for any purpose other than Government procurement does not in any way obligate the U.S. Government. The fact that the Government formulated or supplied the drawings, specifications, or other data does not license the holder or any other person or corporation; or convey any rights or permission to manufacture, use, or sell any patented invention that may relate to them.

This report was cleared for public release by the Air Force Research Laboratory Wright Site (AFRL/WS) Public Affairs Office and is available to the general public, including foreign nationals. Copies may be obtained from the Defense Technical Information Center (DTIC) (<http://www.dtic.mil>).

AFRL-VA-WP-TP-2007-311 HAS BEEN REVIEWED AND IS APPROVED FOR PUBLICATION IN ACCORDANCE WITH ASSIGNED DISTRIBUTION STATEMENT.

*//Signature//

Phillip R. Chandler
Senior Aerospace Engineer
Control Design and Analysis Branch
Air Force Research Laboratory
Air Vehicles Directorate

//Signature//

Deborah S. Grismer
Chief, Control Design and Analysis Branch
Air Force Research Laboratory
Air Vehicles Directorate

//Signature//

JEFFREY C. TROMP
Senior Technical Advisor
Control Sciences Division
Air Vehicles Directorate

This report is published in the interest of scientific and technical information exchange, and its publication does not constitute the Government's approval or disapproval of its ideas or findings.

*Disseminated copies will show “//Signature//” stamped or typed above the signature blocks.

REPORT DOCUMENTATION PAGE

Form Approved
OMB No. 0704-0188

The public reporting burden for this collection of information is estimated to average 1 hour per response, including the time for reviewing instructions, searching existing data sources, gathering and maintaining the data needed, and completing and reviewing the collection of information. Send comments regarding this burden estimate or any other aspect of this collection of information, including suggestions for reducing this burden, to Department of Defense, Washington Headquarters Services, Directorate for Information Operations and Reports (0704-0188), 1215 Jefferson Davis Highway, Suite 1204, Arlington, VA 22202-4302. Respondents should be aware that notwithstanding any other provision of law, no person shall be subject to any penalty for failing to comply with a collection of information if it does not display a currently valid OMB control number. **PLEASE DO NOT RETURN YOUR FORM TO THE ABOVE ADDRESS.**

1. REPORT DATE (DD-MM-YY) February 2007		2. REPORT TYPE Conference Paper Preprint		3. DATES COVERED (From - To) 06/01/2006 – 02/01/2007	
4. TITLE AND SUBTITLE A REVIEW OF RECENT ALGORITHMS AND A NEW AND IMPROVED COOPERATIVE CONTROL DESIGN FOR GENERATING A PHANTOM TRACK (PREPRINT)				5a. CONTRACT NUMBER In-house	
				5b. GRANT NUMBER	
				5c. PROGRAM ELEMENT NUMBER 61102F	
6. AUTHOR(S) Keith B. Purvis (University of California) Phillip R. Chandler (AFRL/VACA)				5d. PROJECT NUMBER A03D	
				5e. TASK NUMBER	
				5f. WORK UNIT NUMBER 0B	
7. PERFORMING ORGANIZATION NAME(S) AND ADDRESS(ES) University of California Dept. of Mechanical Engineering Santa Barbara, CA 93106-5070				8. PERFORMING ORGANIZATION REPORT NUMBER AFRL-VA-WP-TP-2007-311	
Control Design and Analysis Branch (AFRL/VACA) Control Sciences Division Air Vehicles Directorate Air Force Materiel Command, Air Force Research Laboratory Wright-Patterson Air Force Base, OH 45433-7542					
9. SPONSORING/MONITORING AGENCY NAME(S) AND ADDRESS(ES) Air Vehicles Directorate Air Force Research Laboratory Air Force Materiel Command Wright-Patterson Air Force Base, OH 45433-7542				10. SPONSORING/MONITORING AGENCY ACRONYM(S) AFRL-VA-WP	
				11. SPONSORING/MONITORING AGENCY REPORT NUMBER(S) AFRL-VA-WP-TP-2007-311	
12. DISTRIBUTION/AVAILABILITY STATEMENT Approved for public release; distribution unlimited.					
13. SUPPLEMENTARY NOTES Conference paper submitted to the Proceedings of the 2007 American Control Council Conference. This is a work of the U.S. Government and is not subject to copyright protection in the United States. PAO Case Number: AFRL/WS 07-0435 (cleared February 28, 2007). Paper contains color.					
14. ABSTRACT For a team of unmanned aerial vehicles (UAVs) to deceive a radar network by generating a phantom track requires a high degree of cooperation due to: 1) dynamic constraints imposed mainly by the UAVs and 2) strong coupling caused by the phantom. We first review three works that have addressed this problem, namely two one-step look-ahead algorithms and an optimal solution with full time horizon; original simulations of each are included. Second, since the one-step algorithms do not satisfy the UAV and/or phantom constraints in many cases, we design a new algorithm that does, as shown by simulation. Finally, we add a multi-step look-ahead for the UAV constraints and modify the algorithm so that an operator can dynamically add objective waypoints for the phantom.					
15. SUBJECT TERMS Space Access Vehicle, Control Allocation, Guidance and Control					
16. SECURITY CLASSIFICATION OF:			17. LIMITATION OF ABSTRACT: SAR	18. NUMBER OF PAGES 14	19a. NAME OF RESPONSIBLE PERSON (Monitor) Phillip R. Chandler
a. REPORT Unclassified	b. ABSTRACT Unclassified	c. THIS PAGE Unclassified			

A Review of Recent Algorithms and a New and Improved Cooperative Control Design for Generating a Phantom Track

Keith B. Purvis

Dept. of Mechanical Engineering
University of California
Santa Barbara, CA 93106–5070, USA
kpurvis@engineering.ucsb.edu

Phillip R. Chandler

U.S. Air Force Research Laboratory
Control Design and Analysis Branch
Wright-Patterson AFB, OH 45433-7531
phillip.chandler@wpafb.af.mil

Abstract—For a team of unmanned aerial vehicles (UAVs) to deceive a radar network by generating a phantom track requires a high degree of cooperation due to: 1) dynamic constraints imposed mainly by the UAVs and 2) strong coupling caused by the phantom. We first review three works that have addressed this problem, namely two one-step look-ahead algorithms and an optimal solution with full time horizon; original simulations of each are included. Second, since the one-step algorithms do not satisfy the UAV and/or phantom constraints in many cases, we design a new algorithm that does, as shown by simulation. Finally, we add a multi-step look-ahead for the UAV constraints and modify the algorithm so that an operator can dynamically add objective waypoints for the phantom.

I. INTRODUCTION

This work addresses the problem thoroughly introduced in [1]. Figure 1 illustrates what is desired: A team of unmanned aerial vehicles (UAVs) to deceive an enemy radar network by electronically generating a phantom track of a nonexistent vehicle. A UAV with such a capability will be called an Electronic Combat Air Vehicle (ECAV) throughout.

Due to the task of generating a phantom track and the state-dependent nonlinear constraints on the ECAVs and phantom, there exists a strong coupling between the ECAVs. In other words, the actions of one drastically affect the allowable actions of almost all the others. In the midst of this coupling, our goal is to develop a cooperative control algorithm to guide the ECAVs and phantom that will: 1) readily permit online implementation, 2) satisfy all constraints, and 3) allow the ECAVs to influence the phantom based on local objectives.

Two other algorithms have already been designed for this problem, [2]-[3] and [4], and so we first review these and compare them with a benchmark optimal solution based on [5]. We then design a new and improved algorithm, which is simulated for comparison with the previous ones. Finally, we add a multi-step look-ahead for the ECAV constraints based on solutions to an ODE model of what the algorithm is doing.

II. PRELIMINARIES

We consider, as in [1], a constant-elevation scenario. Some of the key variables are shown in Fig. 2a. Two other important variables are $\phi := \varphi - \theta$ and $\phi_T := \varphi_T - \theta$. For the deception tactic to work, we need one ECAV per radar, and each ECAV must stay on the line of sight (LOS) and between its radar

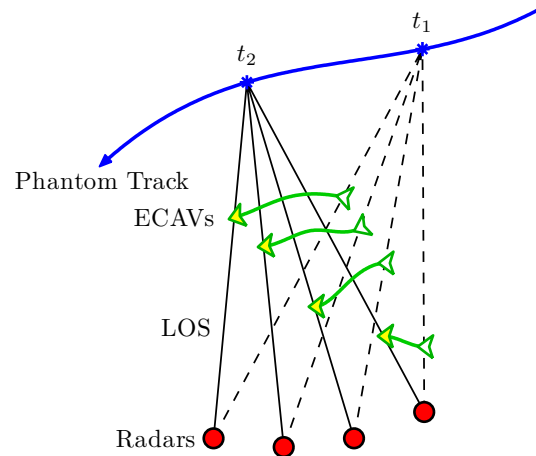


Fig. 1. Deception of a four-radar network by phantom track generation.

and the phantom target. Moreover, the ECAV and phantom are constrained in speed:

$$v_{\min} \leq v(r, \varphi, \theta) \leq v_{\max} \quad (1)$$

$$v_{T\min} \leq v_T \leq v_{T\max} \quad (2)$$

For a given value of θ , which is determined by the phantom track, Fig. 2b represents (1) as feasible heading sectors for the ECAV, which change dramatically with r , θ , and the speed limits. Contrary to [1], [5] but like [2], [3], [4], we plan not to explicitly incorporate the antenna constraints on the ECAV:

$$\phi_{\min} \leq \varphi - \theta(t) \leq \phi_{\max} \quad (3)$$

However, since (3) is generally only violated when the phantom heads approximately toward/away from a radar, we suggest that to satisfy (3), the phantom line of direction be kept sufficiently away from all radars. Finally, the ECAV and phantom are also constrained in acceleration and turn rate; for our algorithm, we decouple the two by constraining speed rate instead of acceleration. The phantom's constraints are imposed to make it believable to the radar network and to keep it from outmaneuvering the ECAVs. This plethora of limitations poses a challenge to finding even a feasible phantom track in many situations, let alone an "optimal" one.

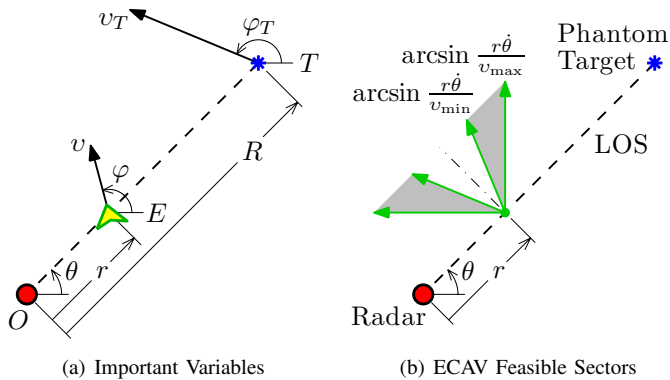


Fig. 2. Illustrations for the deception problem.

III. A REVIEW OF PREVIOUS ALGORITHMS

A. Maithripala and Jayasuriya

The main idea used in [2] is to project the ECAV speed constraints onto the phantom and intersect these projections with the phantom's speed constraints annulus to get the next-step feasible region for the phantom. To simplify computation and guarantee feasibility, each ECAV's projection is converted to a critical phantom angle, which further reduces the feasible region if the ECAV comes too close to the phantom; however, this guarantee no longer holds once the ECAV dynamics are considered. The phantom heading and speed are then determined by taking the point in its feasible region nearest the desired waypoint. The communication required is each ECAV's critical phantom angle with orientation. Turn rates for the ECAVs and phantom are later incorporated in [3] by altering the projections and annulus described above, but this comes after the main development of the algorithm since it ruins the feasibility guarantee.

The approach of using a critical phantom angle is simple, but too conservative. As soon as an ECAV's projection does not allow the phantom to take any heading at *maximum* speed, the critical phantom angle begins restricting the feasible region. This simplification neglects the freedom allowed if instead the phantom's *minimum* speed were used when checking with the ECAV's projection. Consequently, the relative ranges $\frac{r}{R}$ at which an ECAV can fly parallel with the phantom are reduced from $[\frac{v_{\min}}{v_{T\max}}, \frac{v_{\max}}{v_{T\min}}]$ to $[\frac{v_{\min}}{v_{T\max}}, \frac{v_{\max}}{v_{T\max}}]$, which is significantly less than half of the first set for $\pm 20\%$ variation in both the ECAV and phantom speeds.

Since the phantom guidance law always chooses the heading and speed bringing it closest to the desired waypoint, the phantom will generally travel at (constant) maximum speed until the last step, which translates to further loss of freedom in adjusting to meet the ECAV constraints.

The ECAV guidance law suffers from a high gain. Given its feasible headings for the next step, the ECAV tries to move as close as permitted to $\frac{r}{R} = \frac{v_{\text{nom}}}{v_T}$, where v_{nom} is the nominal/average ECAV speed. Although tracking this relative range is a good idea, moving straight toward it at the next step is not prudent and can produce large overshoot given

the ECAV's turn rate, which causes unnecessary infeasible situations. Also, the ECAV acceleration is not limited.

Overall, Maithripala and Jayasuriya's algorithm is too conservative giving poor performance, does not have a good ECAV guidance law, and does not incorporate the ECAV acceleration, which is actually more limiting than its turn rate for this problem. However, the useful contribution here is to project the ECAV constraints onto the phantom and so obtain a next-step feasible region for the phantom.

B. Mears and Akella

In [4], the authors use an optimization approach with the phantom heading as the global decision variable and each ECAV's speed as a local decision variable; the phantom speed is assumed constant. The cost function is composed of six terms to: 1) penalize changes in the phantom heading, 2) keep the phantom headed toward the desired waypoint, 3) minimize ECAV speed, 4) maximize the time an ECAV can generate the phantom track with given heading, 5) minimize rapid ECAV maneuvers, and 6) penalize switching between dynamical systems. Each ECAV computes this cost—optimized over its feasible speeds. The cost functions are then communicated and combined to find the optimal phantom heading for the next step. The fourth term in the cost is actually computed by integrating ahead for an ECAV trajectory until some constraints are violated. Thus, a multi-step look-ahead to help each ECAV stay feasible is buried in the cost function.

Perhaps most disconcerting is the fact that the phantom and ECAV turn rates as well as the ECAV acceleration cannot be limited. Some of these constraints are addressed indirectly in the cost, but this provides no guarantee that they will be even close to satisfied. Furthermore, with so many terms and corresponding weights in the cost function, it is unclear what is really being optimized.

Some freedom is also taken away by constraining the phantom speed to a constant, which could otherwise be helpful in accommodating the ECAV constraints.

Overall, Mears and Akella's algorithm seems impractical since vehicle dynamics can be violated by an arbitrary amount and the heading of the phantom track depends unpredictably on a complex cost function. A useful contribution is the concept of a multi-step look-ahead for avoiding constraints.

C. Purvis, Åström, and Khammash

In [5], the problem is set up as one of Optimal Control and converted into a finite dimensional constrained optimization problem using control parametrization. The horizon is the final time (currently fixed), so the whole phantom track and all vehicle trajectories are determined given the initial conditions, which must be communicated. The control variables are turn rate for the ECAVs and turn rate and linear acceleration for the phantom. The controls can easily be constrained if necessary; explicit constraints can also be added for (3). The integrated cost weights ECAV range and turn rate as well as phantom turn rate, and a final cost is included to make the phantom track terminate near the desired waypoint.

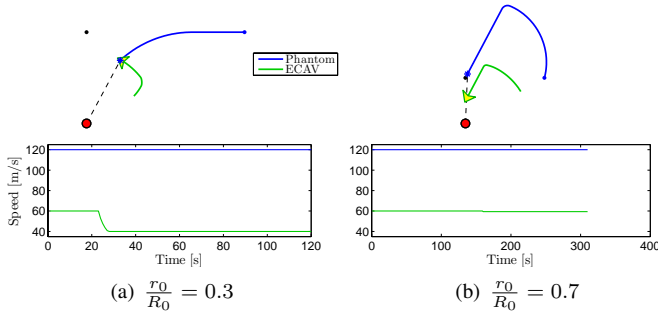


Fig. 3. Simulation results for Maithripala and Jayasuriya’s algorithm, with ECAV and phantom turn rate limits set to approximately $5^\circ/\text{s}$.

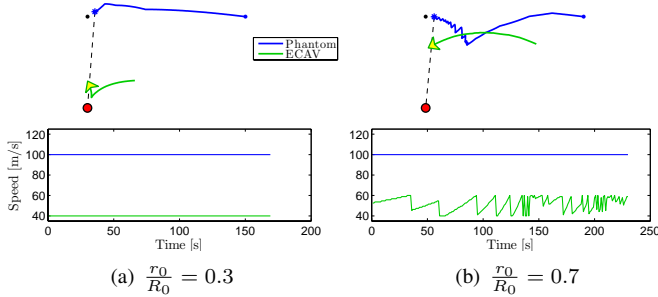


Fig. 4. Simulation results for Mears and Akella’s algorithm, with no ECAV or phantom turn rate limits available.

If used as an online algorithm, this method would require that each ECAV communicate its position and heading, and cooperatively follow its trajectory given by the results of the team optimization. This structure does not allow for any feedback based on local “disturbances” to an ECAV, i.e. it does not permit an ECAV to influence the phantom track through its own local cost function.

Overall, since Purvis, Åström, and Khammash’s solution is optimal over the entire time interval, it provides a nice benchmark to compare more heuristic one-step look-ahead algorithms like those described above. It may also be used online if the information structure is acceptable.

D. Simulations

Upon acquiring and debugging the code for the first two algorithms, we were able to produce verifiable and comparable simulations. Although the algorithms were designed for multiple radars/ECAVs, one radar/ECAV was enough to excite most of the interesting behaviors. The first simulation scenario has the ECAV starting close to the radar, and the second has the ECAV starting close to the phantom. Since it is strategically desirable, the phantom range rate is toward the radar in both scenarios. The ECAV and phantom speeds are both allowed to vary by $\pm 20\%$ unless otherwise constrained by the algorithm.

The simulations for Maithripala and Jayasuriya’s algorithm in Fig. 3 ran quite fast (one or two seconds). On the left, the phantom is forced to curve in toward the radar until it crosses the ECAV. This failure could have been avoided if the

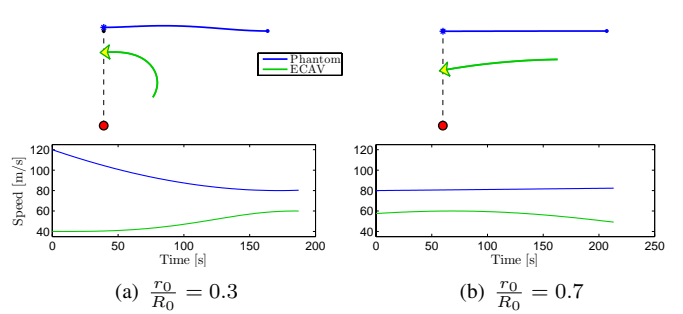


Fig. 5. Benchmark optimal solution from Purvis, Åström, and Khammash’s work, with unconstrained ECAV and phantom turn rates well below $5^\circ/\text{s}$.

ECAV had started out at a slower speed and the phantom had decreased its speed as the ECAV approached. Note also the rapid unlimited ECAV deceleration. On the right, the phantom does reach the waypoint, but only after an extreme unnecessary diversion from the nominal course. This poor performance is due to the conservative nature of the critical phantom angles and the phantom guidance law as discussed earlier.

The simulations for Mears and Akella’s algorithm in Fig. 4 ran slow (several minutes). On the left, the ECAV heading is basically discontinuous toward the end of its trajectory. On the right, the phantom heading and ECAV speed are discontinuous or have extremely large unattainable rates. As stated earlier, it is difficult to interpret the behavior of the phantom and ECAV in light of the cost function because of its complexity.

The simulations for the optimal solution in Fig. 5 ran moderately fast (15 to 30 seconds), though not configured for an optimal solve time. Both solutions look reasonable. On the left, the phantom track is almost straight, and the ECAV trajectory has just enough curvature. The ECAV and phantom speeds fluctuate to help the ECAV get turned around within its constraints. On the right, the phantom actually does not have to turn at all. Again, the ECAV and phantom speeds are appropriate to help the ECAV move away from the phantom.

IV. A NEW AND IMPROVED ALGORITHM—FIRST GENERATION

After reviewing the previous cooperative control algorithms for this problem, it became clear that a new algorithm was needed with a better chance of working in reality. This one-step look-ahead algorithm is a first attempt.

A. An Overview of the Structure

The algorithm runs in MATLAB[®] and consists of one main program, which has all the inputs such as radar positions, starting point and waypoint for the phantom, and initial ECAV ranges. The program calls four subroutines to: 1) compute for each ECAV the information it would communicate to the others, 2) compute the feasible region for the phantom, 3) decide φ_T and v_T for the phantom, and 4) decide φ for each ECAV. These decisions are then used to update the phantom and ECAV positions inside a while loop. The loop runs until the phantom reaches the waypoint or one of several breaking

conditions are met, such as the feasible region becomes empty. In practice, an identical copy of the whole program would run on each vehicle with communication between ECAVs as the only interface.

Assuming that feasible regions have been determined, the general idea is to first choose the phantom heading to go toward the waypoint, except when an ECAV gets too close, which activates “gamma mode.” Secondly, choose the phantom speed to suit the min and max ECAV ranges. Finally, choose a preferred sector for the ECAV heading, and aim toward a secondary waypoint in line with the radar and phantom waypoint.

B. Communication and Construction of the Feasible Region

Based on its speed and angle limits for the next time step (these limits come from respective speed rate and turn rate constraints), an ECAV computes the sector—referenced to its radar—where it can get to in the next step. The sector is characterized by a pair of angles, θ_{\min} and θ_{\max} , which are communicated to the other ECAVs. If the ECAV is too close to the phantom or $\frac{r}{R} \geq \frac{v_{\max}}{v_{T\min}}$, it also computes and sends an angle $\gamma < \pi$ with reference to θ , where

$$\gamma = \arcsin\left(\frac{v_{\max}}{\bar{v}_{T\min}} \frac{R}{r}\right) + \arcsin\left(\frac{v_{\max} dt}{r}\right) \quad (4)$$

(the bar over a speed limit means it is a limit for the next step as opposed to an absolute limit). This angle defines an additional sector for the phantom, $[\theta - \gamma, \theta + \gamma]$, which must be intersected with its feasible region. The basic function of γ is to keep the phantom headed away from any ECAVs that get too close to it. The condition for sending a restricting γ means that, without any speed or angle limits, the ECAV’s sector defined by θ_{\min} and θ_{\max} does not permit the phantom to take certain headings. If this condition is not activated, then the ECAV simply sends $\gamma = \pi$. Assuming that, in gamma mode, the phantom takes heading $\theta \pm \gamma$, it is beneficial to allow the ECAV a small sector of feasible headings instead of just that corresponding to v_{\max} . Therefore, a relaxation is made for the above mathematics:

$$v_{\max} \rightarrow s_v v_{\min} + (1 - s_v) v_{\max} =: v_s, \quad 0 \leq s_v \leq \frac{1}{2} \quad (5)$$

Given θ_{\min} , θ_{\max} , and γ for each ECAV, the feasible region for the phantom is determined by using computational geometry to intersect the ECAV sectors, the phantom’s annulus defined by its next-step speed limits (from speed rate constraints), the phantom’s sector defined by its next-step angle limits (from turn rate constraints), and any sectors coming from restrictive γ ’s. The phantom’s turn rate and speed rate limits are required to be less than or equal to those for each ECAV so that the phantom cannot outmaneuver the ECAVs. Figure 6 illustrates how the feasible region for the phantom is composed, without considering γ . This idea comes from [2], [3], although the authors did not consider incremental speed limits as a way to incorporate speed rate constraints.

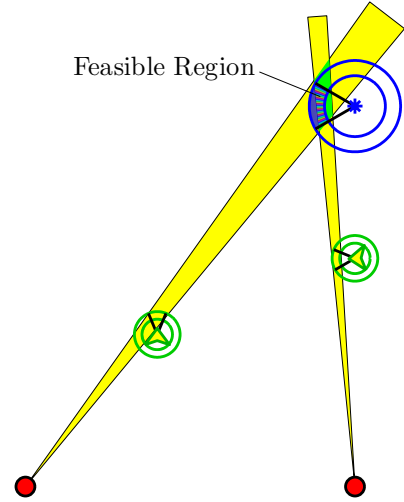


Fig. 6. Composition of the feasible region for the phantom given its next-step speed limits (annulus) and angle limits (sector) and those for two ECAVs.

C. The Phantom Guidance Law

Both the phantom’s speed and heading must be chosen. First, a heading is chosen that crosses the feasible region, and then a speed is chosen from those feasible according to the chosen heading. Choice of these variables, φ_T and v_T , within the feasible limits is made as close as possible to some optimal values, φ_T^* and v_T^* . The optimal heading points from the phantom’s current position to the desired waypoint. The optimal speed is set so that, for the min and max ECAV ranges $\frac{r}{R}$, there are equal ranges on both sides that permit flight parallel to the phantom. However, this speed must not exceed that necessary for the ECAV with the largest range to have a small sector of headings allowing it to decrease its range as needed; this sector should correspond to that provided by γ at the transition out of gamma mode. Therefore,

$$v_T^* = \min \left[\frac{v_{\min} + v_{\max}}{(r/R)_{\min} + (r/R)_{\max}}, \frac{v_s}{(r/R)_{\max}} \right], \quad (6)$$

where v_s is defined by (5). This part of the guidance law ensures that v_T is chosen to best accommodate all the ECAVs, with special attention given to the ECAV closest to the phantom. However, this well-performing law comes at a cost: each ECAV needs to know the ranges of the others. Providing this information through communication may not be desirable; an alternative would be to use the information already communicated to *estimate* the ECAV ranges, similar to the concept in [6].

D. The ECAV Guidance Law

Once the phantom heading and speed are decided, each ECAV must then choose its own heading. Since the phantom is aiming for a waypoint, T_f , it seems natural to guide the ECAV using a waypoint as well, which would provide lo-gain tracking with less overshoot than that used by Maithripala and

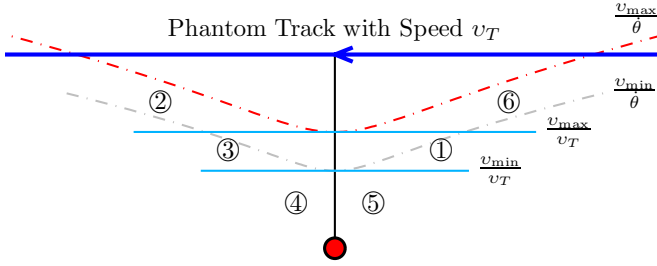


Fig. 7. Division of the ECAV flyable range into six regions, used to determine the preferred ECAV sector to choose from.

TABLE I
ECAV PREFERRED SECTORS FOR THE REGIONS IN FIGURE 7

Region(s)	Condition(s)	Preferred ECAV Heading Sector
①	$\frac{v_{\min}}{v_T} \leq \frac{r}{R} \leq \frac{v_{\max}}{v_T}$ $\cos \phi_T < 0$	closer to radar ^a
②	$\gamma < \pi$ ^b	conservative: further from radar aggressive: closer to radar
③–⑤	not ① or ②	further from radar
⑥	none ^c	not applicable

^a See Fig. 2b to understand the designations “closer” and “further.”

^b Since $\gamma < \pi$ whenever $\frac{r}{R} \geq \frac{v_{\max}}{v_T^{\min}}$ or the ECAV is in regions ② or ⑥, and since the sector defined by γ essentially maps ⑥ to ②, this condition corresponds to region ② (exact when $v_s = v_{\max}$).

^c Region ⑥ won’t be occupied because gamma mode maps ⑥ to ②.

Jayasuriya’s algorithm. The waypoint we use is

$$E_f = \frac{v_{\min} + v_{\max}}{v_{T\min} + v_{T\max}}(T_f - O), \quad (7)$$

where O is the radar position. The optimal heading φ^* points from the ECAV’s current position to E_f , unless gamma mode is active for any ECAV; in this case, $\varphi^* = \varphi_T$, i.e. the ECAV should try to fly parallel with the phantom to follow its maneuvers. Moving toward E_f should make the ECAV approach the range that, when flying parallel to the phantom moving at nominal speed, would have the ECAV fly at its nominal speed. Thus, φ^* should guide the ECAV to the middle of its speed constraints over time.

In general, an ECAV will have a feasible sector of headings on both sides of the heading corresponding to $r\dot{\theta}$ as shown in Fig. 2b, so a preferred sector is chosen that should be used if possible. This choice is based on R , φ_T , and v_T of the phantom, as well as the ECAV speed constraints. The idea here is to try to help the ECAV stay within its constraints in the future and to keep it from getting sucked in to the radar. Figure 7 shows the six regions used in deciding what sector to prefer. The regions, conditions used to identify them, and the preferred ECAV sectors are organized in Table I.

Using its preferred sector of headings defined by its next-step speed limits (coming from speed rate constraints), the ECAV picks the heading closest to φ^* , which points at E_f .

E_f need not be at the left end of region ③ in Fig. 7; it can be pretty much anywhere when gamma mode is activated, which provides part of the motivation for the preferred sector. If the preferred sector does not intersect with its next-step angle limits (coming from turn rate constraints), then the ECAV has no choice but to try the other sector. Note that, in Table I, two choices are given for region ②; the conservative option guarantees that the ECAV will not get sucked in to the radar, but the aggressive option provides better performance on average, i.e. the phantom does not have to turn away from the waypoint as sharply. Observing Fig. 7, it is best to keep the ECAV in regions ① and ③ because this corridor or “sweet spot” is the only area that will allow the ECAV to fly parallel with the phantom in the long term.

In the case that the phantom heads exactly toward or away from the radar, φ is still well chosen based on Table I. If the phantom heads toward the radar, then the ECAV will be in regions ① or ⑤. From the table, $\varphi = \pi + \theta$ if in ①, and $\varphi = \theta$ if in ⑤. If the phantom heads away from the radar, then the ECAV will be in regions ②, ③, or ④, and the table gives $\varphi = \theta$ for all three regions when the conservative choice is used for ② (the aggressive choice is not too bad either, since the ECAV would be heading toward the radar but starting at a large distance from it). However, in this special case, it is not enough to choose φ ; v must also be chosen, and it is based here on whether the phantom and ECAV are aimed toward or opposing each other:

$$v = \begin{cases} \min [\bar{v}_{\max}, \max (\bar{v}_{\min}, \frac{r}{R} v_T)] & \cos(\varphi - \varphi_T) < 0 \\ \bar{v}_{\min} & \cos(\varphi - \varphi_T) > 0 \end{cases} \quad (8)$$

In the general case, once φ is chosen, v may be calculated using

$$v = \frac{r \sin d\theta}{dt \sin(\phi - d\theta)} \quad (9)$$

provided $d\theta := \theta^+ - \theta \neq 0$ or $\text{mod}(\phi, \pi) \neq 0$. Equation (9) is analogous to $v = r\dot{\theta}/\sin \phi$ for continuous time.

In working toward a guarantee that the ECAV will never get sucked in to the radar with this guidance law, it is useful to consider what happens in the transitions between regions. This analysis is ongoing. However, one thing is clear: the γ -mapping from ⑥ to ② is discontinuous after $t = 0$. In other words, if an ECAV enters region ⑥ from ①, it will switch from $\gamma = \pi$ to something given by (4) and generally less than $\frac{\pi}{2}$. Hence, gamma mode will fail in most cases to redirect the phantom track because the sector $[\theta - \gamma, \theta + \gamma]$ won’t intersect with that defined by the phantom’s turn rate constraints. One situation already apparent where this would come up is when an ECAV starts in region ⑤ and has to make a large turnaround before it can fly parallel with the radar. One way to address this problem would be to calculate multiple steps ahead and see if the ECAV would be able to reach parallel flight with the phantom in the sweet spot without hitting any constraints.

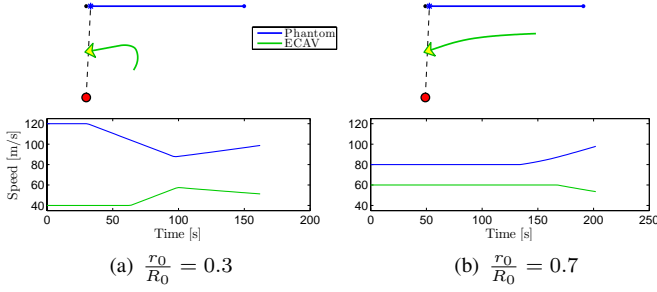


Fig. 8. Simulation results for the new algorithm, with ECAV and phantom turn rate limits set to $5^\circ/\text{s}$ and ECAV and phantom speed rates set to $0.05 \text{ g}'\text{s}$.

E. Simulations

For completeness, the new algorithm is applied to the same two scenarios in Fig.'s 3, 4, and 5, and the simulations are shown in Fig. 8. Comparing the figures, the new algorithm performs much better than the previous one-step look-ahead algorithms in Fig.'s 3 and 4, even with all pertinent dynamic constraints included; indeed, the simulations in Fig. 8 appear very similar to the optimal solution in Fig. 5.

V. A LOOK-AHEAD FOR AN ECAV CLOSE TO ITS RADAR

A multi-step look-ahead is now developed for an ECAV starting close to its radar when the phantom range rate is toward the radar. To begin, we seek to understand and model in continuous time what the ECAV actually does using its guidance law above when starting in region ⑤ of Fig. 7.

A. General Analysis

Given a phantom track, a simple model that describes an ECAV's free motion in terms of its speed is

$$\dot{r} = \begin{cases} +\sqrt{v^2 - (r\dot{\theta})^2} \\ -\sqrt{v^2 - (r\dot{\theta})^2} \end{cases}, \quad (10)$$

where only the + or - is solved at a given time, and switching between solutions requires the quantity inside the root to be zero—see [1] for details. This model is relevant because an ECAV trying to make a turnaround will generally be limited by its speed rate as opposed to its turn rate. For a straight constant-speed phantom track, we have:

$$\dot{\theta} = \frac{1}{R} v_T \sin \phi_T \quad (11)$$

$$\dot{R} = v_T \cos \phi_T \quad (12)$$

To reduce the three-state system given by (10)–(12), first substitute (11) for $\dot{\theta}$ in (10):

$$\dot{r} = \begin{cases} +\sqrt{v^2 - \left(\frac{r}{R} v_T\right)^2 \sin^2 \phi_T} =: f^+ \\ -\sqrt{v^2 - \left(\frac{r}{R} v_T\right)^2 \sin^2 \phi_T} =: f^- \end{cases} \quad (13)$$

Next, define the new state $\frac{r}{R} v_T$ and differentiate:

$$\frac{d}{dt} \left(\frac{r}{R} v_T \right) = \left[\frac{1}{R} \dot{r} - \frac{r}{R^2} \dot{R} \right] v_T + \frac{r}{R} \dot{v}_T \quad (14)$$

Using (12), f^+ from (13), $\dot{v}_T = 0$ (constant speed phantom), and $R = \frac{R_{\min}}{\sin \phi_T}$ (straight phantom track) in (14), we get

$$\frac{d}{dt} \left(\frac{r}{R} v_T \right) = \frac{v_T}{R_{\min}} \sin \phi_T \left[f^+ - \left(\frac{r}{R} v_T \right) \cos \phi_T \right], \quad (15)$$

and since $\dot{\phi}_T = -\dot{\theta}$ (straight phantom track), (11) becomes

$$\frac{d\phi_T}{dt} = -\frac{v_T}{R_{\min}} \sin^2 \phi_T. \quad (16)$$

Finally, dividing (15) by (16) yields

$$\frac{d}{d\phi_T} \left(\frac{r}{R} v_T \right) = -\csc \phi_T \left[f^+ - \left(\frac{r}{R} v_T \right) \cos \phi_T \right], \quad (17)$$

which is a one-dimensional dynamical system with state $\frac{r}{R} v_T$, independent variable ϕ_T , and control v that completely describes the evolution of the ECAV's relative range (scaled by v_T) in space when its range rate is toward the phantom.

B. A Model for the Actual ECAV Guidance Law

The actual ECAV guidance law turns the ECAV as sharply as permitted at all times until parallel flight with the phantom is reached; first, this is limited by v_{\min} and then by \dot{v}_{\max} . Figure 9 makes this idea more concrete by showing an ECAV trajectory, which is a solution of three different ODEs modeling what the guidance law actually dictates (for a straight constant-speed phantom track). In addition, the ECAV trajectory shown is critical in the sense that any trajectory starting with a larger range would not be able to make a successful turnaround. Segment A of the trajectory solves

$$\frac{d}{d\phi_T} \left(\frac{r}{R} v_T \right) = -\csc \phi_T \left[f^+(v_{\min}) - \left(\frac{r}{R} v_T \right) \cos \phi_T \right] \quad (18)$$

$$\left(\frac{r}{R} v_T \right) (\phi_{T0}) = \left(\frac{r}{R} v_T \right)_0 \quad (19)$$

$$\left(\frac{r}{R} v_T \right) (\phi_{T1}) = \frac{v_{\min}}{\sin \phi_{T1}}, \quad (20)$$

where $f^+(v_{\min})$ is just f^+ from (13) with $v = v_{\min}$, and the end condition (20) corresponds to $r\dot{\theta} = v_{\min}$. The ODE for segment A is just (17) with $v = v_{\min}$. Segment B of the trajectory solves

$$\frac{d}{d\phi_T} \left(\frac{r}{R} v_T \right) = -\csc \phi_T \left[f^-(\bar{v}) - \left(\frac{r}{R} v_T \right) \cos \phi_T \right] \quad (21)$$

$$\bar{v}(\phi_T) = \dot{v}_{\max} \frac{R_{\min}}{v_T} (\cot \phi_T - \cot \phi_{T1}) + v_{\min} \quad (22)$$

$$\left(\frac{r}{R} v_T \right) (\phi_{T2}) = \bar{v}(\phi_{T2}), \quad (23)$$

where $f^-(\bar{v})$ is just f^- from (13) with $v = \bar{v}(\phi_T)$, which comes from integrating $\dot{v}/\dot{\phi}_T$ with $\dot{\phi}_T$ given by (16). Observing (21)–(22), we see that segment B depends on the initial value ϕ_{T1} . Note that if the quantity under the root in f^- ever goes negative, then the integration stops because of infeasibility (\dot{v}_{\max} is not sufficient to match the increasing rate of $r\dot{\theta}$). Segment C of the trajectory solves

$$\frac{d}{d\phi_T} \left(\frac{r}{R} v_T \right) = 0 \quad (24)$$

$$\left(\frac{r}{R} v_T \right) (\phi_{Tf} = \frac{\pi}{2}) = v_{\max}. \quad (25)$$

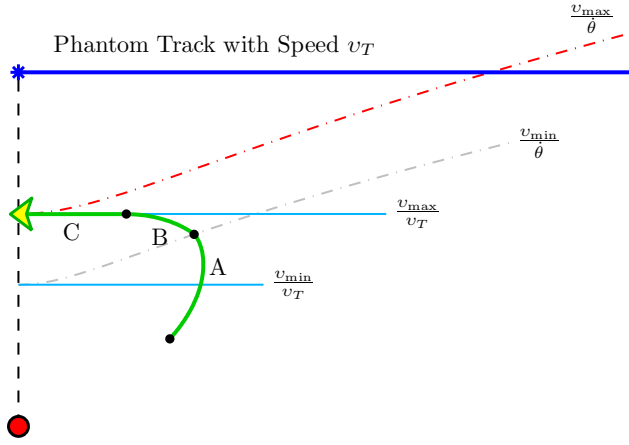


Fig. 9. Trajectory an ECAV would follow using its guidance law for a given initial range and angle that start it below the “sweet spot.”

What makes this whole pursuit worthwhile is that any ECAV trajectory defined by the above model and having a lesser range than the critical trajectory for *some* ϕ_T is feasible. This fact follows from the existence and uniqueness of the solutions described by (18)–(25), which must be shown. It is straightforward to show that the right-hand sides of (18), (21), and (24) are Lipschitz continuous for relevant $\frac{r}{R}v_T$ and $\phi_T \in [\varepsilon, \pi - \varepsilon]$ (except at transition points), which is required by the Existence and Uniqueness Theorem. Careful examination of the transitions also shows that no trajectory crossovers are possible.

Assuming that the ECAV’s speed and speed rate constraints are fixed, observe that (18)–(25) depend only on $\frac{r}{R}v_T$, ϕ_T , and $\frac{R_{\min}}{v_T}$. In fact, only segment B depends on the last term; this time parameter matters only when \dot{v}_{\max} plays a role or is limiting. Using shooting, (18)–(25) can be integrated to get the critical ECAV trajectories for a variety of $\frac{R_{\min}}{v_T}$ values—see Fig. 10. This figure was used to predict critical ECAV trajectories for the actual algorithm, and the results agreed quite accurately—within half a degree or better. Using standard 2-D interpolation, an ECAV can determine for a given ϕ_T and $\frac{R_{\min}}{v_T}$ whether or not it will make a successful turnaround. If infeasibility is predicted, then the phantom heading should be modified by slightly decreasing ϕ_T . This change will move the ECAV to the left in Fig. 10 and to a higher $\frac{R_{\min}}{v_T}$ -curve. However, decreasing ϕ_T may not be possible when the ECAV is on segment B because the increased speed rate required may be outside the constraints (in this case, the best course is no action).

Observing Fig. 10, the critical ECAV trajectories for lower $\frac{R_{\min}}{v_T}$ values do not even achieve v_{\max} at $\phi_T = 90^\circ$. This result is caused by the small bound on \dot{v} . Physically, what happens is that when the ECAV transitions to segment B (see Fig. 9), \dot{v} begins to have a tug-of-war with $\frac{d}{dt}(r\dot{\theta})$ while $\dot{\theta}$ is significantly increasing. The requirement for feasibility is

$$\dot{v} \geq \frac{d}{dt}(r\dot{\theta}) = \dot{r}\dot{\theta} + r\ddot{\theta}. \quad (26)$$

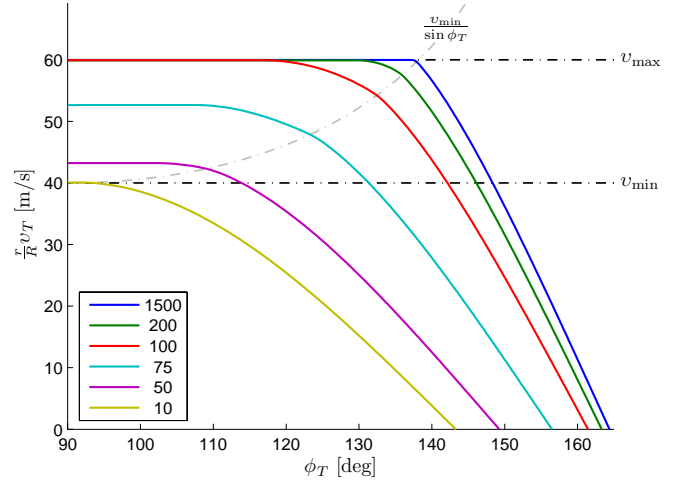


Fig. 10. $\frac{r}{R}v_T$ versus ϕ_T of the critical ECAV trajectories for different values of $\frac{R_{\min}}{v_T}$, with $\dot{v}_{\max} = 0.05$ g’s.

Since r is nonincreasing after segment A, we have $\dot{r} \leq 0$. This implies a simple requirement on the ECAV’s speed rate limit:

$$\dot{v}_{\max} \geq r\ddot{\theta} \quad (27)$$

The right-hand term has a complicated dependence on both the phantom track and the ECAV motion, which depends on its guidance law. Therefore, r_{\max} and $\ddot{\theta}_{\max}$ are found separately to get an upper bound. First, $\ddot{\theta}$ is determined by differentiating (11) with φ_T and v_T constant:

$$\begin{aligned} \ddot{\theta} &= \frac{-R\dot{\theta}v_T \cos \phi_T - \dot{R}v_T \sin \phi_T}{R^2} \\ &= -2\frac{v_T^2}{R_{\min}^2} \sin^3 \phi_T \cos \phi_T \end{aligned} \quad (28)$$

Differentiating again and setting equal to zero gives $\phi_{T\max} = \frac{2\pi}{3}$ for $\phi_T \in [0, \pi]$. Plugging $\phi_{T\max}$ back into (28) yields

$$\ddot{\theta}_{\max} = \frac{3\sqrt{3}}{8} \frac{v_T^2}{R_{\min}^2} \quad (29)$$

To find r_{\max} given that the ECAV is starting in region ⑤ of Fig. 7, Fig. 9 suggests that on segment B the largest possible range is where $\frac{v_{\max}}{v_T} = \frac{v_{\min}}{\dot{\theta}}$. Solving this equation,

$$r_{\max} = \frac{v_{\max}^2}{v_{\min}} \frac{R_{\min}}{v_T}. \quad (30)$$

Using r_{\max} and $\ddot{\theta}_{\max}$ in (27) and rearranging now gives

$$\left(\frac{R_{\min}}{v_T}\right)_{\min} = \frac{3\sqrt{3}}{8} \frac{v_{\max}}{\dot{v}_{\max}} \frac{v_{\max}}{v_{\min}}, \quad (31)$$

which is the (conservative) minimum value of $\frac{R_{\min}}{v_T}$ that will not cause infeasibility due to \dot{v}_{\max} (infeasibility could still occur due to v_{\max}). Using the same ECAV constraints as specified in Fig. 10, (31) gives 120 as the minimum for $\frac{R_{\min}}{v_T}$; as expected, this is a little high since the curve for $\frac{R_{\min}}{v_T} = 100$ still achieves v_{\max} in the figure.

VI. THE SECOND-GENERATION ALGORITHM

A. Changes to the Existing Design

The first change to our algorithm is that the initial relative ranges an ECAV can start from are now bounded above by $\frac{v_s}{v_{T\min}}$ so that the old gamma mode based on (4) is no longer needed (it is only useful when activated at $t = 0$ as discussed earlier). Our reasoning is that little is gained by placing an ECAV closer to the phantom, which then causes the phantom to veer off on a long gradual curve before heading toward the waypoint. If an ECAV can start close to the phantom, then it should be able to turn slightly, fly down closer to its radar, and begin generating a nice *straight* phantom track a few seconds later. In addition, infeasible configurations can be created when multiple ECAVs are too close to the phantom and their LOS's are significantly spread apart in angle. Thus, placing an upper bound on where an ECAV can start makes the problem simpler and sacrifices little in terms of realistic limitations.

The second change to the algorithm is the determination of v_T^* , which before required knowledge of the ECAV ranges. Now, each ECAV communicates its choice for v_T , and the minimum of these values is taken for v_T^* . This change decreases the performance somewhat but has the advantage that the ECAVs have some direct influence over the phantom speed.

B. Addition of the Look-Ahead

Using data similar to that in Fig. 10 but with a finer grid, a 2-D interpolation now allows an ECAV starting in region ⑤ of Fig. 7 to check whether the current phantom heading and speed will allow a successful turnaround into the sweet spot. If not, then the ECAV computes and sends a *new* γ , which is just the current ϕ_T decreased by a fraction of the phantom's next-step angle limits. There are a few situations where the ECAV's γ may not be feasible for other ECAVs in the same predicament. In this case, the current solution is to then disregard all γ 's in constructing the feasible region for the phantom.

C. Addition of Dynamic Objective Waypoints

An operator can now dynamically update the objective waypoint for the phantom. *Objective* waypoint is stressed because, as these points are added, the phantom immediately focuses on the newest point without regard for previous "waypoints." This construction is similar to a receding horizon, where the current objective waypoint is the horizon. To allow the ECAVs to follow the phantom's maneuver to a new objective waypoint, φ^* is temporarily set to φ_T . The ECAVs must then wait until all are flying parallel with the phantom (and have communicated so) before the phantom can begin turning toward the new objective waypoint. When the algorithm begins, this wait time can be several time steps, but later on it's immediate since the ECAVs have converged to their optimal ranges given by E_f .

D. Simulations

An example of the second-generation algorithm in action for 3 radars is given in Fig. 11. Two dynamic objective waypoints are specified. For the first, the look-ahead is activated by the ECAV on the right, which turns the phantom to a less acute

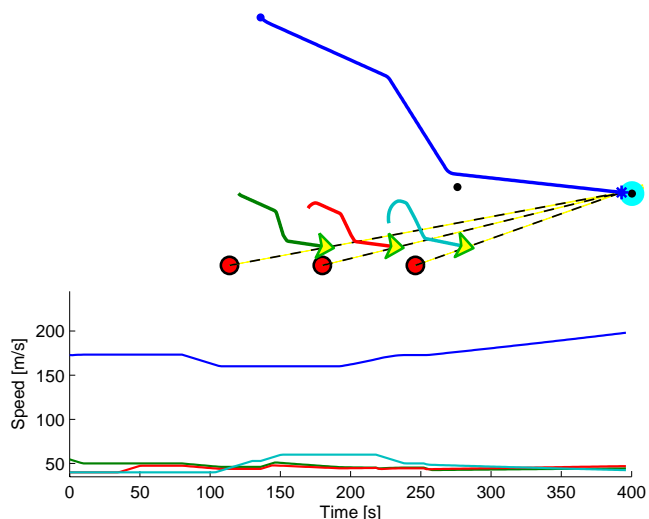


Fig. 11. Simulation results for the new algorithm—second generation—for a 3-radar scenario, with the nominal phantom speed set to 4x the ECAVs'.

heading until that ECAV can accommodate the phantom heading directly toward the objective waypoint. As time increases, the speeds begin approaching their nominal values.

VII. CONCLUSIONS AND FUTURE WORK

Given the complexity and high coupling of the phantom track problem, the new algorithm developed herein is quite robust and provides a solid base for future development. The next pressing addition should be a tracking controller that would guide any ECAV forced off its LOS by constraints to track back onto the LOS in minimum time. Given this capability, a better decision process should be implemented to deal with the case when one ECAV's γ is not feasible for another ECAV. Adding an estimator for the ECAV states based on communicated information would also aid the algorithm's performance—specifically by providing better information for selecting the phantom speed. Finally, analysis should be conducted to determine what happens and what can be done when one of the ECAVs experiences a communication outage.

REFERENCES

- [1] K. B. Purvis, P. R. Chandler, and M. Pachter, "Feasible flight paths for cooperative generation of a phantom radar track," *AIAA Journal of Guidance, Control, and Dynamics*, vol. 29, no. 3, pp. 653–661, May–June 2006.
- [2] D. H. A. Maithripala and S. Jayasuriya, "Radar deception through phantom track generation," in *Proc. of the American Control Conf.*, vol. 6, June 2005, pp. 4102–4106.
- [3] D. H. A. Maithripala, "Radar deception through phantom track generation," Master's thesis, Texas A&M University, 2006.
- [4] M. J. Mears and M. R. Akella, "Deception of radar systems using cooperatively controlled unmanned air vehicles," in *Proc. of the IEEE International Conf. on Networking, Sensing, and Control*, March 2005, pp. 332–335.
- [5] K. B. Purvis, K. J. Åström, and M. Khammash, "Practical methods for highly coupled cooperative uavs," in *American Control Conf.*, New York City, July 2007.
- [6] T. Shima, P. R. Chandler, and M. Pachter, "Decentralized estimation for cooperative phantom track generation," in *Proc. of the 5th International Conf. on Cooperative Control and Optimization*. River Edge, NJ: World Scientific, January 2005.